TU Dortmund

Case Studies

Project 2: BTA Deep Hole Drilling

Lecturers:

Dr. Uwe Ligges

M. Sc. Marie Beisemann

M. Sc. Leonie Schürmeyer

Author: Tadeo Hepperle

Group number: 5

Group members:

Lennard Heinrigs, Tadeo Hepperle,
Joshua Oehmen, Vanlal Peka

July 26, 2023

Contents

1 Introduction

BTA deep hole drilling is a machining process that is used to drill deep holes. A deep hole is a hole with a relatively large depth to diameter ratio. BTA stands for Boring and Trepanning Association. BTA drilling techniques can be used to create holes with a diameter of 6 mm to 1500 mm (VDI-Richtlinie 3210, 1996, p. 4). The material which is processed is typically metal and a depth to diameter ratio of up to 400:1 can be achieved (UNISIG GmbH, 2023). In contrast to other drilling techniques, usually the workpiece rotates around the drilling head. During the drilling process oil is injected into the drilled hole with high pressure. On the one hand the oil cools down the work piece that is heated up by the boring friction. On the other hand it also sweeps away metal chipping that is removed from the work piece by the BTA boring head.
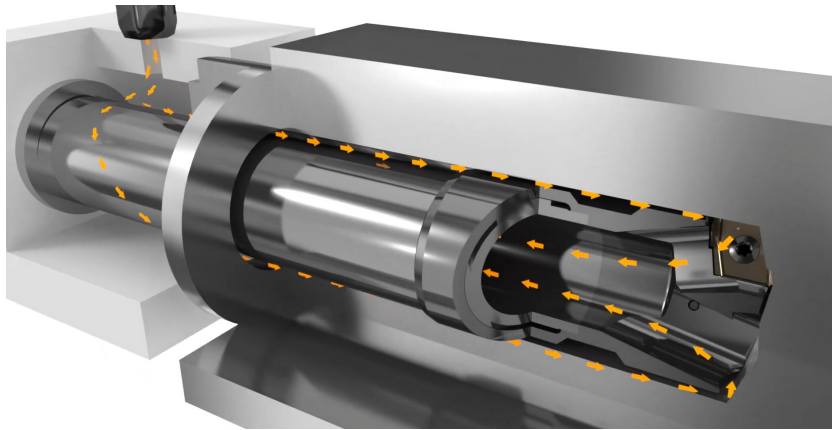

Figure 1: Oil flow in a BTA drilling head (Botek Präzisionsbohrtechnik GmbH, 2023)

The yellow arrows in Figure 1 show the flow of oil in the process. Oil returns together with any removed metal chipping through the center of BTA tool. To support the BTA tool and reduce unwanted vibrations a damper may be used. In this report we take a look at BTA drilling processes with and without a damper. Because the holes in BTA drilling are so deep, the drilling head needs to be quite flexible: A drill that is too stiff could break from torsional forces easily. This flexibility comes at a disadvantage: the drilling head in a BTA machine needs to be self guiding, and it is difficult to make sure that the hole is completely straight on such a long drilling path without any deviance at the hole borders.

The flexible drilling head can develop vibrations which lead to two undesired phenomenons: chatter and spiraling. Chatter can be described as "self-excited torsional vibrations" (Raabe et al., 2010, p. 746). The torsional eigen-frequencies of the drilling
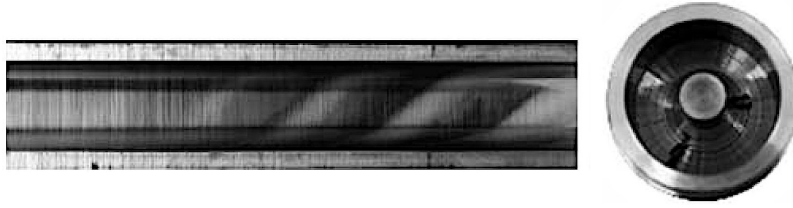
Figure 2: Spiraling (left) and Chatter (right) (Raabe et al., 2010, p. 746)

tool lead to the edge of the drilling head chipping away material in an uneven way. The effect on the work piece can be seen in the right image in Figure 2. Chatter can be heard acoustically as a sort of humming. According to Theis (2004, p. 14), chatter is recognizable by the human ear as a "high-pitched tone which occurs during the process". Spiraling is caused by bending vibrations. The impairment of the borehole can be seen on the left side of Figure 2. We do not have data on whether spiraling occurred in the processes we analyze in this report and will thus not make statements about it. The main objective of this report is to find a good predictor of chatter and develop an early warning system to allow the BTA machine to be turned off before chatter causes too much damage to the work piece.

1.1 Prior Research

We now talk briefly about prior approaches that have been taken to detect chatter. Raabe et al. (2010) propose to model chatter as a regenerative process. They run a chatter simulation that constantly updates the angle of the BTA tool, the cutting thickness and the drilling torque. They found that their physical model produces chatter similar to chatter in real world drilling processes regarding the drilling torque (Raabe et al., 2010, p. 748). Weinert et al. (2001) also experimented with predicting chatter in BTA processes. They found that the drilling torque is one of the most expressive signals for chatter detection. The other variables they looked at are force, acceleration in 3 directions and acoustic signals. Even though chatter can be recognized by pronounced frequencies on the acoustic channel, loud noise of other machinery in the factory makes the acoustic channel an impractical predictor (Weinert et al., 2001, p. 6). They found that the auto-correlation function for the drilling torque differs significantly between *chatter* and *non-chatter* segments of the BTA process. To predict chatter, an absolute sum of the ACF function (A_{ACF}-value) over 30 lags was used. When this value crossed a certain threshold a couple of times, it was a strong indicator of chatter appearing

4

soon after. To find the best decision rule based on the A_{ACF} a neural network was used. Theis (2004, p. 27) also found that the drilling torque is an important predictor of chatter and has shown that the spectrograms of the torque variable differ significantly between *chatter* and *non-chatter* time regions of the BTA process. Because of these findings we also expect the drilling torque (*moment* variable) to be of great use for chatter detection in this report.

1.2 The Data

To answer the question of what causes chatter in BTA boring processes we take a look at data from 10 BTA drilling runs in this report. As shown in Table 1, each process has its own identifier (e.g. *D4*), by which we refer to a process. We refer to the processes *D4*, *D6* and *D8* as *D*-processes, while *V2*, *V6*, *V10*, *V17*, *V20*, *V24* and *V25* are called *V*-processes. The *D*-processes were recorded in 2002 and featured a damper installed in the drilling device, 1240 mm away from clamping. In contrast to that, the *V*-processes were recorded in 2001 and did not use any damper in the BTA machine setup. It seems like the *D*-processes do not show signs of chatter, while we can observe some form of chatter in all *V*-processes.

Table 1: Drilling Processes and their Metadata

identifier	duration	cutting speed	feed speed	oil pressure
D4	3:54 min	111 m/min	0.231 mm/s	unknown
D6	4:28 min	120 m/min	0.185 mm/s	unknown
D8	4:27 min	90 m/min	0.250 mm/s	unknown
V2	4:51 min	120 m/min	0.185 mm/s	unknown
V6	4:25 min	111 m/min	0.231 mm/s	371 l/min
V10	4:25 min	111 m/min	0.231 mm/s	229 l/min
V17	4:44 min	120 m/min	0.185 mm/s	300 l/min
V20	4:58 min	90 m/min	0.250 mm/s	300 l/min
V24	4:29 min	120 m/min	0.185 mm/s	300 l/min
V25	4:33 min	120 m/min	0.185 mm/s	300 l/min

There are a few parameters that are chosen in advance for each drilling process: *cutting speed*, *feed speed* and *oil pressure*. Table 1 shows these parameters for the 10 processes. The data for each of the 10 processes consists of a time series recording of several variables. The time series data was recorded with a sampling rate of 20000Hz, so in each second of the boring process, 20000 observations of each of the measured variables

have been recorded. That means there is no missing data and a consistent time gap of 0.05 ms between measurements. The durations of the drilling process recordings range from 3:54 min to 4:58 min. The data was recorded utilizing the *TEAC GX-1 Integrated Recorder* device, a machine developed by the *TEAC* electronics company. The distribution of the device has been discontinued (DAQLOG Systems Ltd, 2023). The machine features a set of up to 8 input channels that can be fed with analog data. Then, 16-bit A/D (analog to digital) converters convert the analog signals into a digital one, saving the measurement of each channel as a 16-bit signed integer. The associated coefficients to convert the physical value to an integer value and vice versa need to be specified before the recording starts. They can be used to restore continuous physical values from the 16-bit measurements. The data is stored in an *interlaced* format. That means, for each point in time, the 16 bit value measured on each channel is appended to a file. So if we split the resulting file into chunks of $2 * NUMBER\_OF\_CHANNELS$ bytes, each of these chunks represents one point in time.

The following variables were measured for all 10 processes:

- *acoustic* - the audio signal in Pa (Pascal), sound produced during the drilling process by the BTA machine and its surroundings.

- *moment* - the torsional moment in Nm (Newton meter), also known as drilling torque. Measured at the drilling bar above the borehole of the BTA drilling machine. It is created by forces of chipping, friction and deformation at the guide rails.

- *sync signal* - an electric signal that is triggered by the drilling head having a certain axial rotation. It flows once per revolution of the drilling head for a brief moment.

- *oil acceleration* - the acceleration of the drilling oil supply in m/s^2.

- *force* - the force in feed direction in N (Newton). It is related to the *feed speed* but also to the resistance (hardness) the work piece material has against being drilled.

Besides that, the 7 *V*-processes feature 2 additional variables for the acceleration of the drilling head: *lateral acceleration* and *frontal acceleration* (acceleration in frontal direction) each measured in m/s^2. The 3 *D*-processes also contain the *bending moment* in Nm as a variable. They also contain measurements on a variable called "bohrst", but it remains unclear to us what this variable stands for. It is measured in m/s^2 but more we do not know, hence we do not further discuss it in this report.

1.2.1 Labels

The data we received is unlabeled. That means we just have the time series of the predictor variables, but do not know in what time regions chatter appears. The only thing we could do is listen to the audio signal. Because chatter can be heard as a high-pitched tone, we were able to manually label each process and divide it into different time segments:

- *start* - before the boring head made contact to the material.

- *no chatter* - normal drilling, no audible chatter.

- *chatter* - audible chatter, recognizable as consistent high tones in the audio.

- *low chatter* - audible chatter, but the tone is not as high as in the *chatter* section before. Often appears after some time of high tones *chatter*.

- *end* - after the boring head is done with drilling and no pressure is asserted on the material anymore

The time segments appear in each process in this order, sometimes skipping the *chatter* and *low chatter* stages. The main focus of this report is to detect the change from *no chatter* to *chatter* with some procedure that would work online only with data from **before** the *chatter* stage is entered.

2 Methods

This chapter briefly explains the statistical methods used. to apply them we use Python (Rossum and Drake, 2009) as statistical software. The Python packages polars (pola-rs, 2023) and matplotlib (Hunter, 2007) have been used. In addition to these, we developed a custom python package called *gx1convert* (Hepperle, 2023) that was used to read in the header and binary data produced by the GX-1 device.

2.1 Short-time Fourier Transform (STFT)

Short-time Fourier Transform (STFT) is a signal processing method that can be applied to a time series, to translate it from the time domain into the frequency domain. Consider a discrete real valued time series X_t. The STFT is defined as a function $\mathbb{R} \to \mathbb{C}$, mapping

each X_t time point to a function $Y_t(\omega)$ that maps an angular frequency to a complex number. This complex number z can be written in its Euler representation $re^{i\phi}$. We will discuss shortly how to interpret it. $Y_t(\omega)$ can be calculated with the following formula (Smith, 2023):

$$Y_t(\omega) = \sum_{t=-\infty}^{\infty} X_t w(n-m)e^{-j\omega t}$$

In this formula, $w(t)$ represents a window function that is shifted over all possible values of t by an offset of m. A window function is a function that takes values between 0 and 1 in some range and returns 0 outside that range. For the sake of simplicity, this can be thought of as a simple rectangular window, that returns 1 within a fixed range and 0 otherwise. In practice any window function can be used. When using the infinite sum in the formula of $Y_t(\omega)$ on real data, X_t values falling outside the data range have to be replaced by 0. Let $z = re^{i\phi}$ be the complex number that we get, when evaluating $Y_t(\omega)$ for some ω and a fixed point in time t. Then r and ϕ represent the amplitude and phase of a sin wave with angular frequency ω at the time point t. The angular frequency ω can be converted to an actual frequency f of our time series in Hz by $f = \omega\frac{s}{2\pi}$, where s is the sampling frequency of the time series in Hz. Likewise, if we want to know the STFT in a time point t for any frequency f, we can use $\omega = f\frac{2\pi}{s}$ to calculate the corresponding radial frequency ω to pass to the $Y_t(\omega)$ function to obtain amplitude and phase.

The short-time Fourier transform can be used to represent the dominant frequencies of a time series over time with a spectrogram. A spectrogram can be plotted as a heatmap with the time t on the x-axis, the frequency f on the y-axis and the spectrogram value S_{tf} represented by a color on a color spectrum. The spectrogram value S_{tf} for a time point t and a frequency f is defined as the squared magnitude of the STFT: $|Y_t(\omega)|^2 = |Y_t(f\frac{2\pi}{s})|^2$. It can be used to visualize how a frequency distribution in a time series behaves over time.

2.2 Covariance and Correlation

Given a set of n data points each consisting of a value on two metric variables X and Y, their covariance s_{XY} can be computed as the product of the difference to the respective variable mean summed up for all data points and divided by n.

$$s_{XY} = \frac{1}{n} \cdot \sum_{i=1}^{n} (x_i - \overline{x}) \cdot (y_i - \overline{y})$$

It is a measure of how much the variables vary together linearly in the same direction. Because the covariance greatly depends on the units of measurement, it can be standardized to a range between -1 and $+1$ by dividing it by the standard deviations of both variables.

$$r_{XY} = \frac{s_{XY}}{s_X \cdot s_Y}$$

The result r_{XY} is known as Pearson's r or Pearson product-moment correlation coefficient. Note that r_{XY} is symmetrical, so $r_{XY} = r_{YX}$ and in case that either s_X or s_Y is zero it is not defined. It is a standardized measure of linear correlation between two metric variables (Eid et al., 2017, p. 538). A correlation of $r_{XY} = 1$ means perfect correlation.

2.3 Auto-correlation Function (ACF)

The auto-correlation function (ACF) shows how much a time series is correlated with a lagged version of itself. For a Time series X_t consisting of n data points $x_1, ..., x_n$ the ACF is defined as a function $\rho(k)$ that maps an integer k to the correlation of X_t with X_{t+k} (Deistler and Scherrer, 2022, p. 4):

$$\rho(k) = Corr(X_t, X_{t+k})$$

In this equation, k represents a lag value. In time series analysis we call a "lag", a shift of the time series along the temporal direction. The correlation is calculated over all possible values of t where $1 \leq t \leq n - k$. For example for values $t = 3$ and $k = 2$, the variable X_t would refer to the data point x_3 and X_t would be x_5. From the equation follows that $\rho(0)$ is always 1, because $\rho(0) = Corr(X_t, X_t) = 1$. Because the ACF for higher lag values has fewer data point pairs available for correlation calculation, one should only calculate the ACF for lag values much less than the length of the time series itself. Interpreting the ACF only makes sense if the underlying process is (weakly) stationary (Deistler and Scherrer, 2022, p. 4). This should be given if we look at regions

of a drilling process where mean and variance do not change too much. Periodicity in a time series also shows as periodic patterns in the ACF.

2.3.1 Absolute Area under the ACF (A_{ACF})

Weinert et al. (2001) derived a value called A_{ACF} from the auto-correlation function. They selected a range of L lags $k \in \{0, ..., L\}$ and calculated the ACF $\rho(k)$ for each lag value. Then they summed up the absolute value for each lag to obtain the A_{ACF}.

$$A_{ACF} = \sum_{k=0}^{L} |p(k)|$$

Weinert et al. (2001) chose a value of L=30 in their approach and calculated this A_{ACF} value for small chunks of time cut out of the original time series. If there are strong resonating frequencies in the data (such as present during chatter), the A_{ACF} value is expected to be high.

3 Data Analysis

We manually labeled each process into segments as described in section 1.2.1. Table 2 shows the time regions we determined for each segment in seconds:

Table 2: Time Segments of each Drilling Process

	start	no chatter	chatter	low chatter	end
D4	0 - 3	3 - 222	/	/	222 - 234
D6	0 - 2	2 - 254	/	/	254 - 268
D8	0 - 4	4 - 254	/	/	254 - 267
V2	0 - 10	10 - 200	200 - 264	/	264 - 291
V6	0 - 31	31 - 47	47 - 136	136 - 253	253 - 265
V10	0 - 31	31 - 47	47 - 91	91 - 252	252 - 264
V17	0 - 16	16 - 35	35 - 45	45 - 270	270 - 284
V20	0 - 33	33 - 52	52 - 136	136 - 287	287 - 298
V24	0 - 3	3 - 22	22 - 64	64 - 258	258 - 269
V25	0 - 5	5 - 118	118 - 260	/	260 - 272

The points where the *chatter* phase starts and ends were identified by listening to the *acoustic* channel. The end point of the *start* segment and the start point of the *end*

segment were best identified by looking at the *force* time series for each process. The force quickly increases (in absolute value) when the BTA drilling head makes contact with the workpiece and falls when it is released, as visible in Figure 21. We also plotted the time series for *moment*, *sync signal*, *oil acceleration* and *acoustic* for all processes together with the time segments. They can be found in Figure 22 to Figure 25 in the Appendix. For the *V*-processes Figure 26 and Figure 27 show the frontal and lateral acceleration respectively. The reason for plotting all of these variables in conjunction with the time segments is, that it helps us identify which variables show a visible difference between the chatter and non-chatter regions. It looks like only the *acoustic* signal and the *moment* and *oil acceleration* show visible differences.

3.1 Frequencies and ACF

We now want to take a look at the frequency space. Figure 3 shows spectrograms for the *V2*-Process. The *V2*-Process shall just serve as an example. The area between the blue and purple line is the *non-chatter* segment, while the area between the purple and blue line marks the *chatter* segment. We can see that *force*, *moment*, *acoustic* and *oil acceleration* show changes in their pattern as soon as the chatter appears. But there does not seem to be a pattern forming, before the chatter starts, as one would hope to conduct predictions based on the patterns.

If we assume that chatter is in general associated with the workpiece resonating certain frequencies, it is not surprising to see patterns to be more pronounced in the *chatter* segment. Some of the spectrograms in Figure 3 show a strong frequency around 670 Hz in the *chatter* segment. Using all data points from the *chatter* and *non-chatter* regions respectively we calculate the ACF up to lag 100 for each variable of the *V2*-process. We are looking for a variable where the ACF differs a lot between *chatter* and *non-chatter* regions. This would allow us then to witness how the ACF changes from its *non-chatter* form to the *chatter* constellation and shut down the machine before we fully reach the *chatter* phase.

Figure 4 and Figure 5 show a very regular periodic pattern in the ACF for the *chatter* phase for the variables *moment* and *oil acceleration*. The wavelength seems to be around 30 lags. Since $20000/30 \approx 667$ this lag constellation would suggest a dominant frequency of around 667 Hz. This is also visible as a thick black horizontal line in the *chatter* region of the top left spectrogram of Figure 3 (*moment* variable) at around this frequency. In the
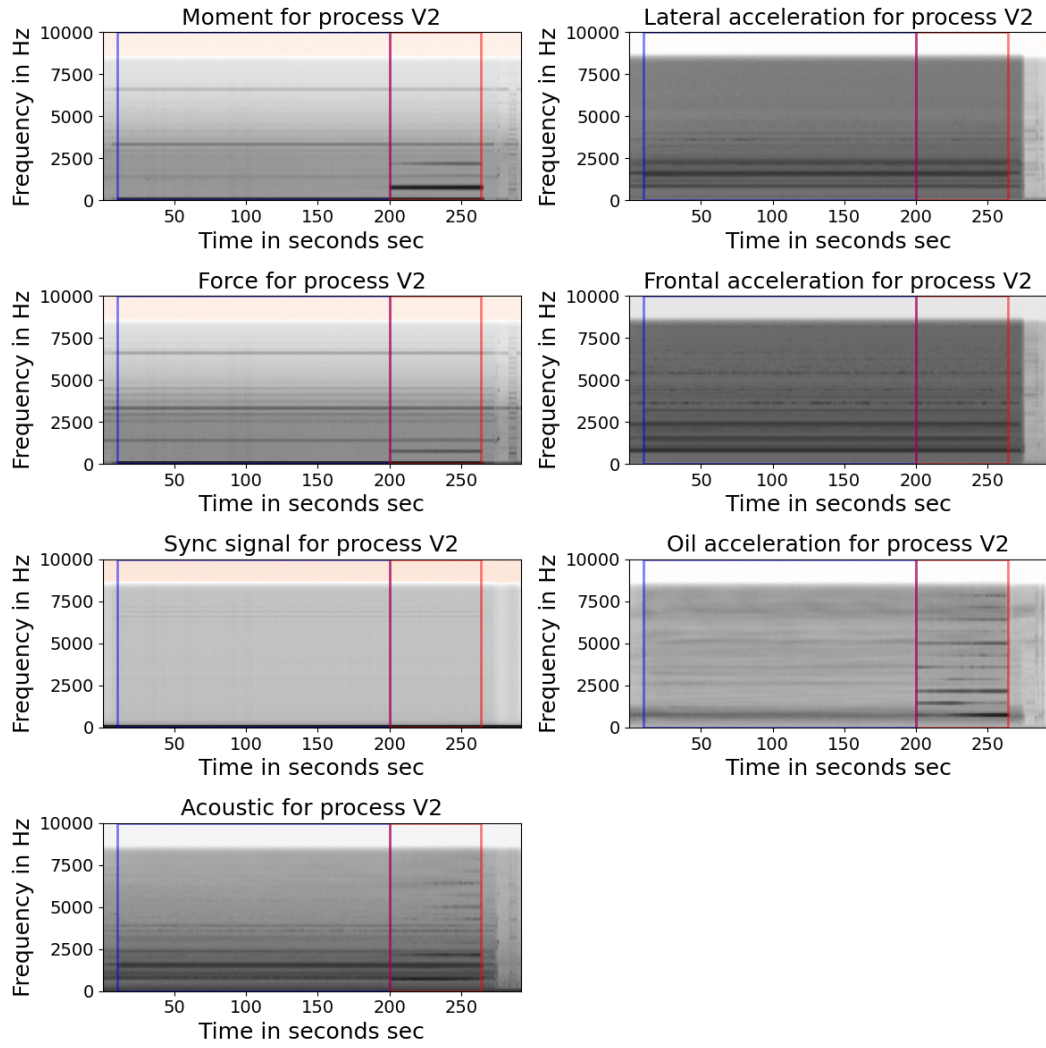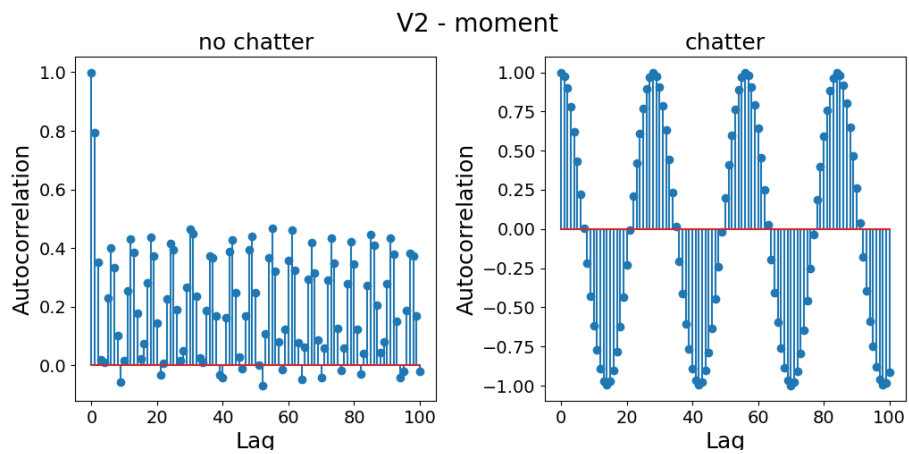
Figure 3: Spectrogram for the *V2*-Process

Figure 4: ACF for the *moment* variable of the *V2* process in two regions

non-chatter regions the behavior of the ACF differs between the two variables though: *oil acceleration* shows some slowly decaying pattern, where after 100 lags almost no correlation is left, while we can observe some high frequent oscillations in the ACF of *moment*.

Figure 7 and Figure 6 show that the ACFs of the *acoustic* and the *force* channel show similar behavior, but the ACF in the *chatter* region is not as regular as in the *moment* channel. The *sync signal*, *lateral acceleration* and *frontal acceleration* variables are probably not very useful to detect chatter: The ACFs for *chatter* vs. *non chatter* segments in Figure 8, 9 and 10 do not really differ. We conclude that the drilling torque (*moment* variable) is probably the best suited predictor, moving forward.

3.2 Detect chatter with A_{ACF}

We now split the time series into chunks with a width of 1000 data points. That is the equivalent of 50 ms for each chunk. For each of these chunks we calculate the ACF up to lag 100. Using a similar approach as Deistler and Scherrer (2022) we reduce these 101 coefficients down to an A_{ACF} value that represents the absolute area under the auto-correlation function: $A_{ACF} = \sum_{k=0}^{L} |\rho(k)|$. Here $\rho(k)$ is the auto-correlation at lag k calculated on the respective 1000-point chunk. Using this approach the *non-chatter* segments had between 320 and 3800 chunks and the *chatter* segments we composed of 200 to 2840 chunks. Table 3 shows for each of the processes the average A_{ACF} values in the *chatter* and *non-chatter* regions.

Table 3: A_{ACF} from ACF up to lag 100 for *moment* in *non-chatter* and *chatter* segments. N = *non-chatter*, C = *chatter*

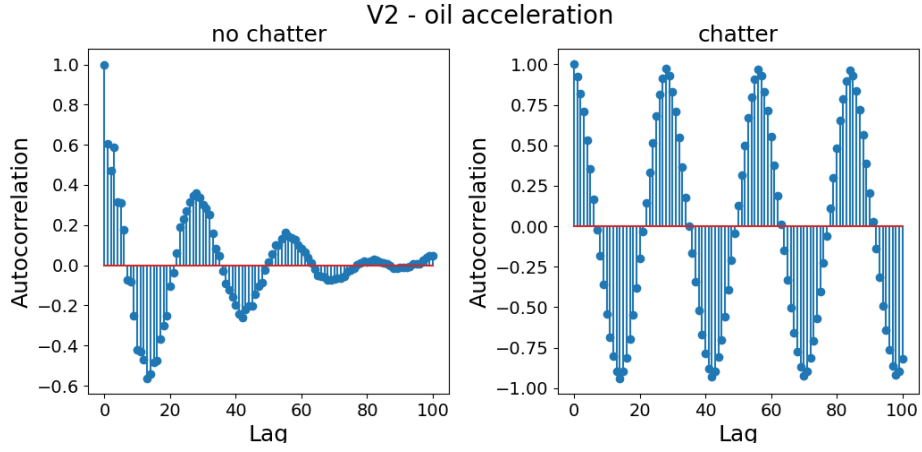| process	mean		std		min		max	
	N	C	N	C	N	C	N	C
D4	12.85		2.54		7.59		44.61	
D6	13.21		4.48		4.59		41.27	
D8	14.45		3.60		5.94		39.38	
V2	19.56	61.54	8.43	0.06	5.79	61.15	60.16	61.73
V6	11.49	60.48	7.04	1.80	5.21	37.51	44.64	61.04
V10	10.88	60.75	5.43	1.16	5.37	33.88	36.69	61.02
V17	16.89	59.57	11.19	3.81	4.99	35.90	61.04	61.29
V20	13.13	58.62	7.54	3.17	5.42	32.63	50.40	61.95
V24	12.23	60.54	8.81	1.81	5.50	39.58	60.90	62.93
V25	21.35	61.09	14.56	0.95	6.02	42.54	60.92	61.68

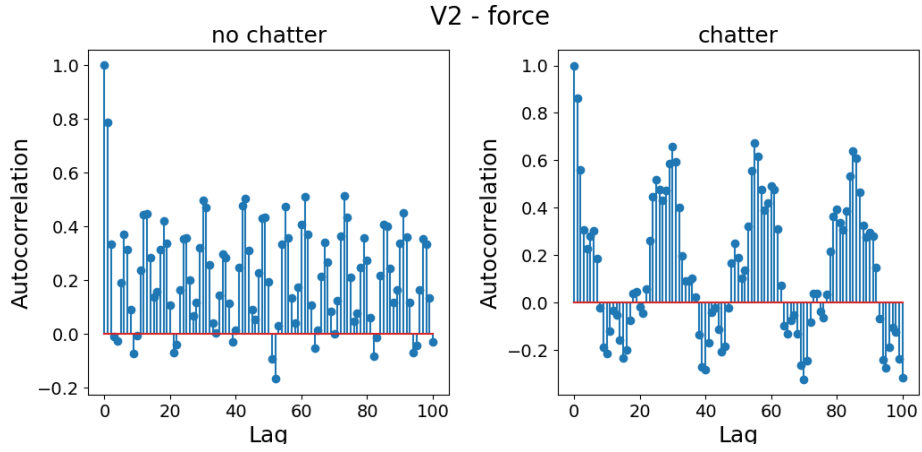Figure 5: ACF for the *oil acceleration* variable of the *V2* process in two regions

Figure 6: ACF for the *force* variable of the *V2* process in two regions
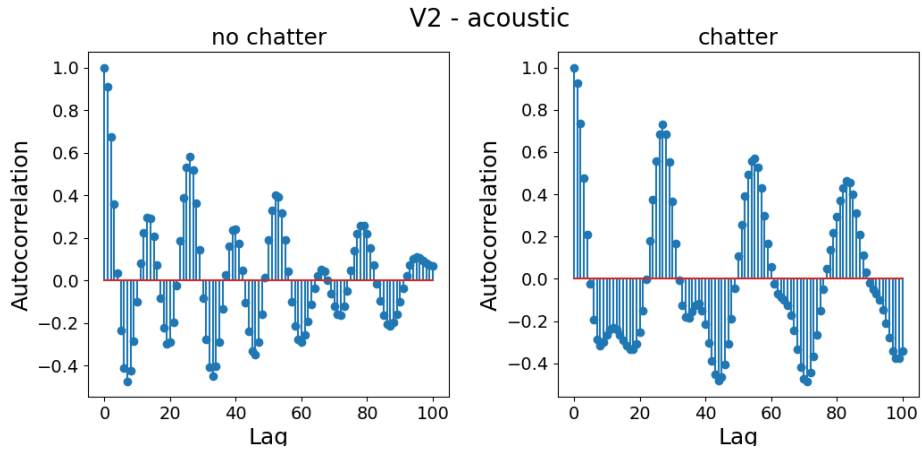

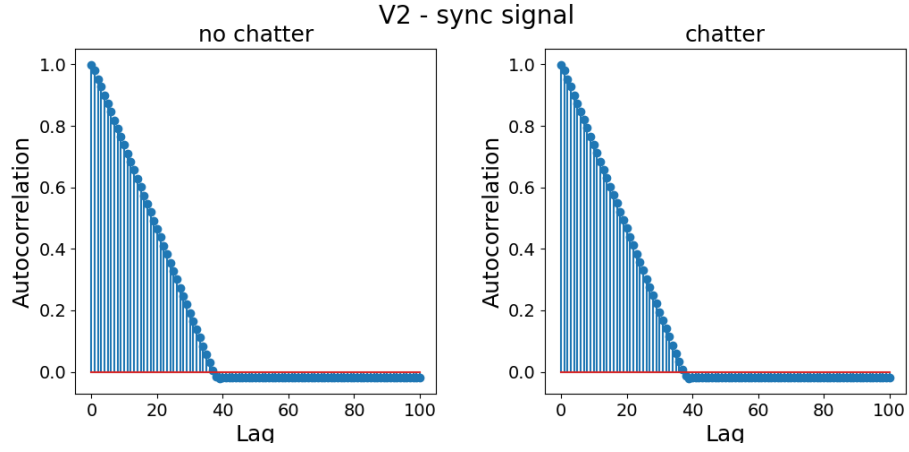Figure 7: ACF for the *acoustic* variable of the *V2* process in two regions

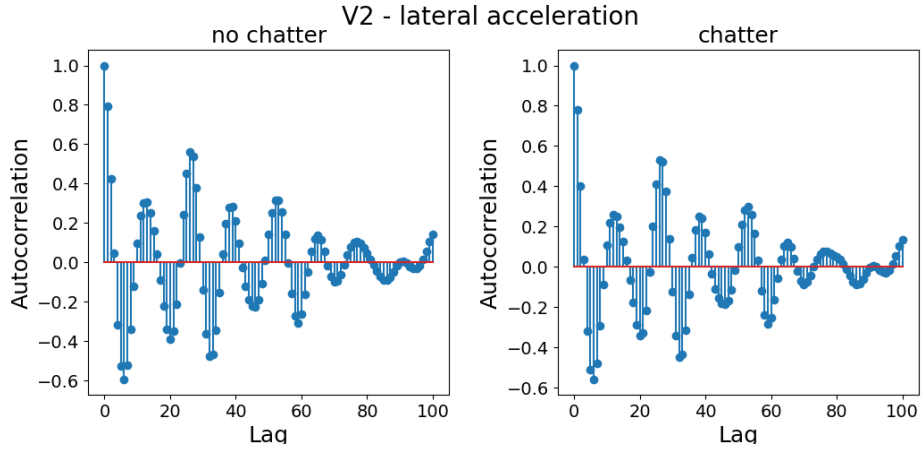Figure 8: ACF for the *sync signal* variable of the *V2* process in two regions

Figure 9: ACF for the *lateral acceleration* variable of the *V2* process in two regions
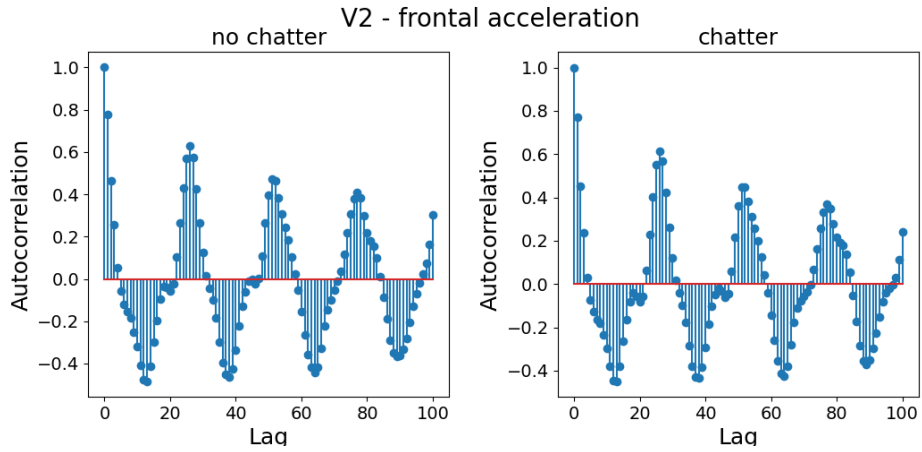

Figure 10: ACF for the *frontal acceleration* variable of the *V2* process in two regions

We can see that all time series show an average A_{ACF} value of around 10 - 21 in the non-chatter regions. Those processes that show chatter have average A_{ACF} values of 58.62 to 61.54 in the chatter regions. That is a large difference. One way to interpret the A_{ACF} values is, as a measure of how much any measured value can be predicted by the preceding 100 values. This however is not very close to the truth, because it does not account for shared predictive variance between different lag values. What Table 3 also shows is, that for all V-processes the variance of the A_{ACF} values is lower in the *chatter* segments than in the *non-chatter* segments. This is not surprising, because chatter is all about structured vibrations occurring for some time, which makes the A_{ACF} be quite uniform across chunks. But it is also true, that some chunks in the *non-chatter* segments have higher A_{ACF} values that some chunks of the *chatter* region of the same process, as the *min* and *max* columns in the table show. So to develop a policy that allows us to detect chatter based on the A_{ACF} value we need to take a closer look at some graphs.

Firstly plotting the A_{ACF} value of the *moment* variable for each chunk of the D-processes shows us that the A_{ACF} varies quite a bit, but never reaches values greater than 45 (See Figure 11, 12 and 13). For all the V-processes we can see a similar behavior of the A_{ACF} when entering the *chatter* region: The A_{ACF} shoots up to a value around 60 and then stays relatively constant for almost the entire *chatter* period. During the *low chatter* segment, that often follows, the A_{ACF} is a bit lower and not so low in variance, but still higher than when no chatter occurs.
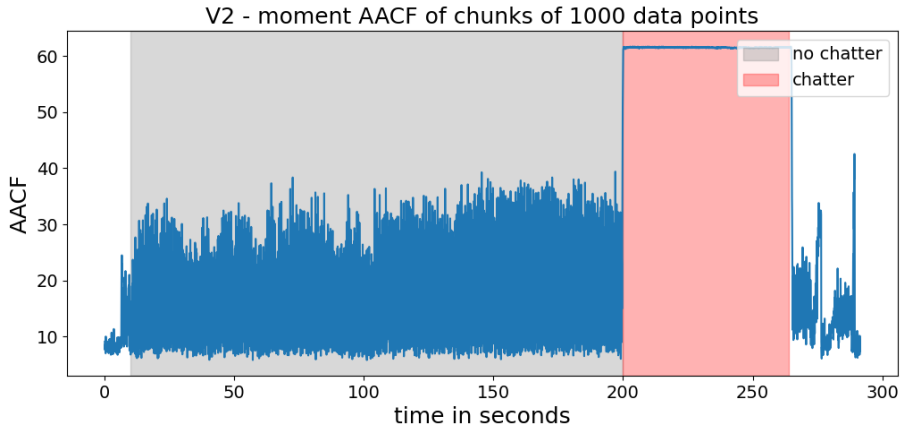

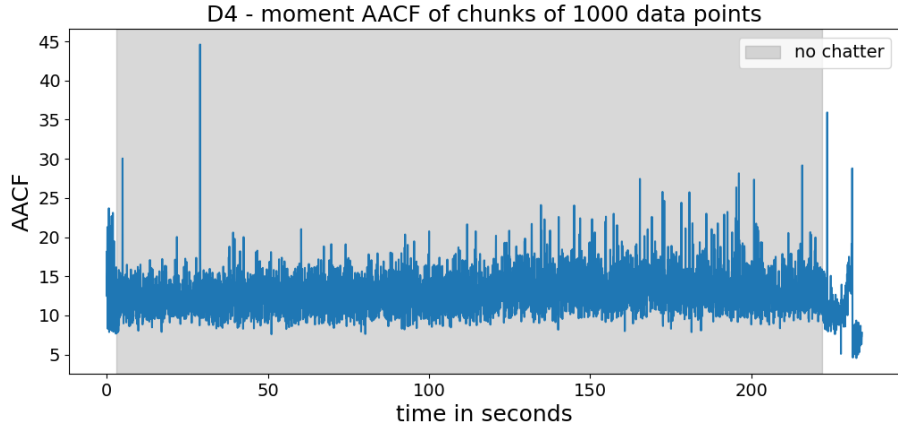Figure 14: *V2* process: A_{ACF} for *moment* variable

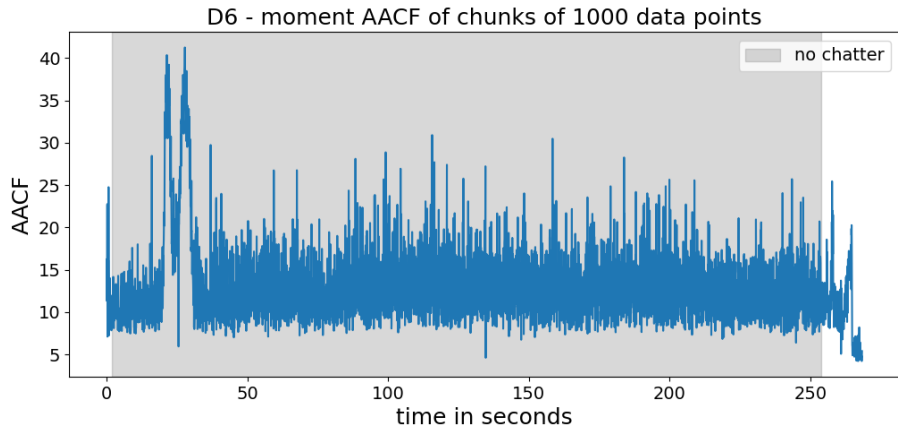Figure 11: *D4* process: A_{ACF} for *moment* variable

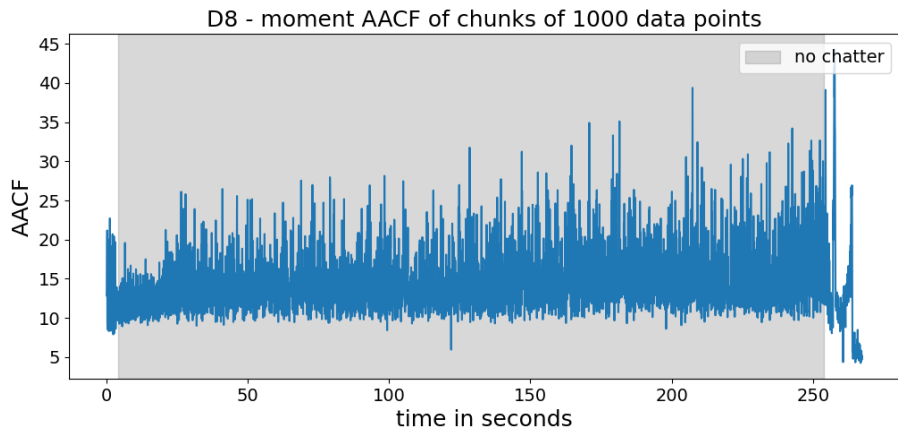Figure 12: *D6* process: A_{ACF} for *moment* variable

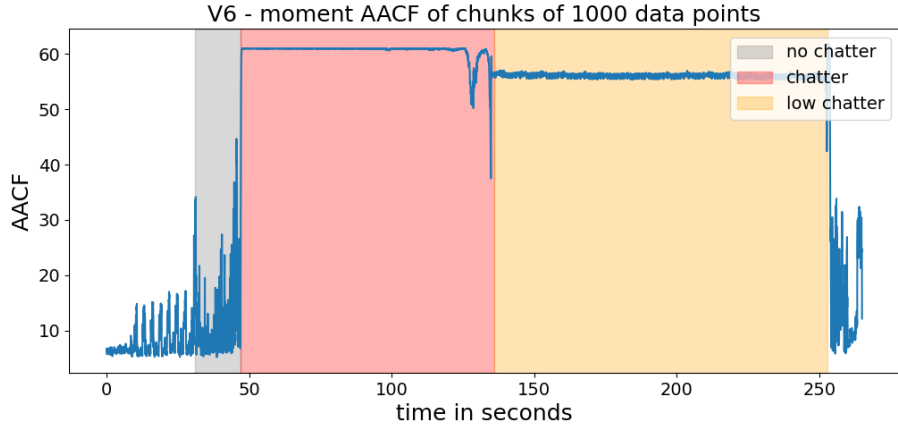Figure 13: *D8* process: A_{ACF} for *moment* variable

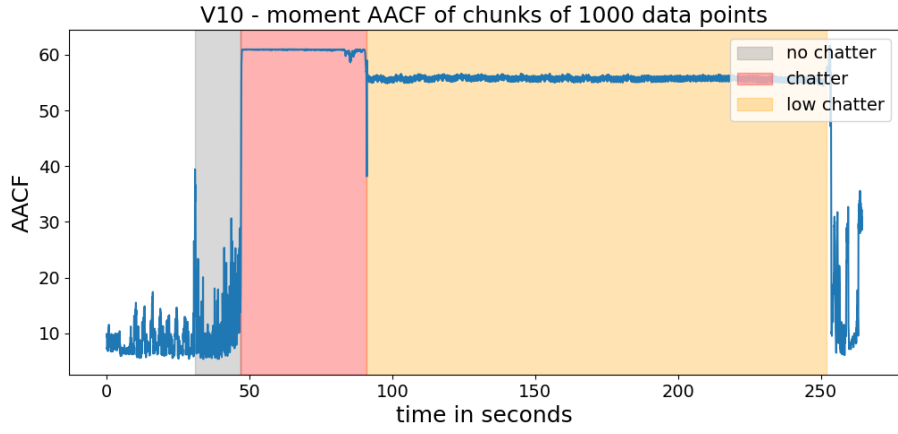Figure 15: *V6* process: A_{ACF} for *moment* variable

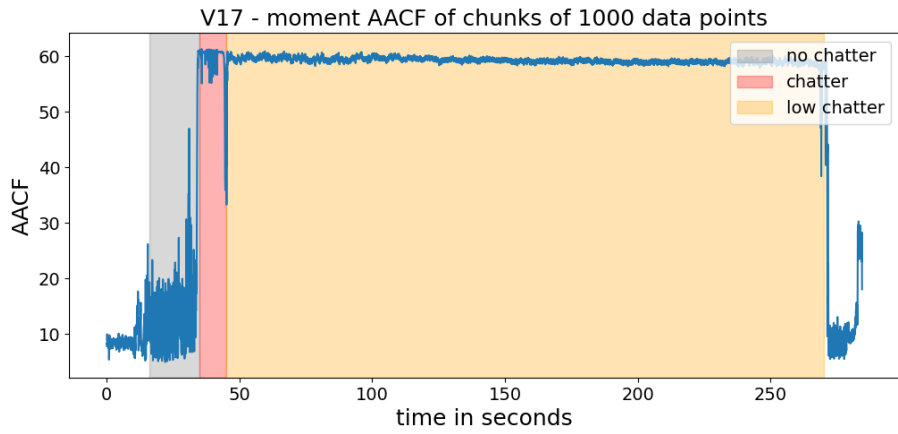Figure 16: *V10* process: A_{ACF} for *moment* variable

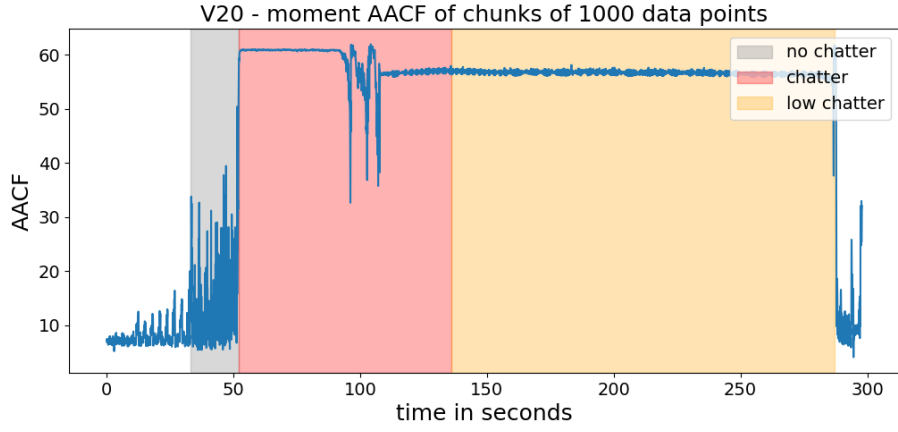Figure 17: *V17* process: A_{ACF} for *moment* variable

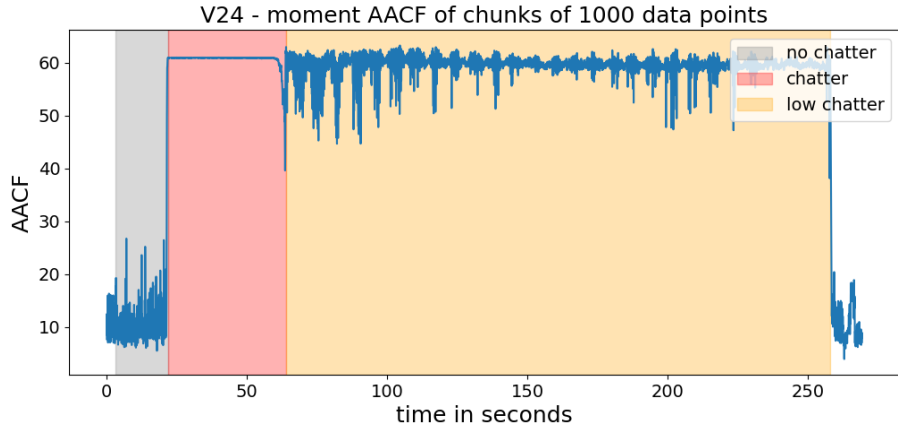Figure 18: *V20* process: A_{ACF} for *moment* variable

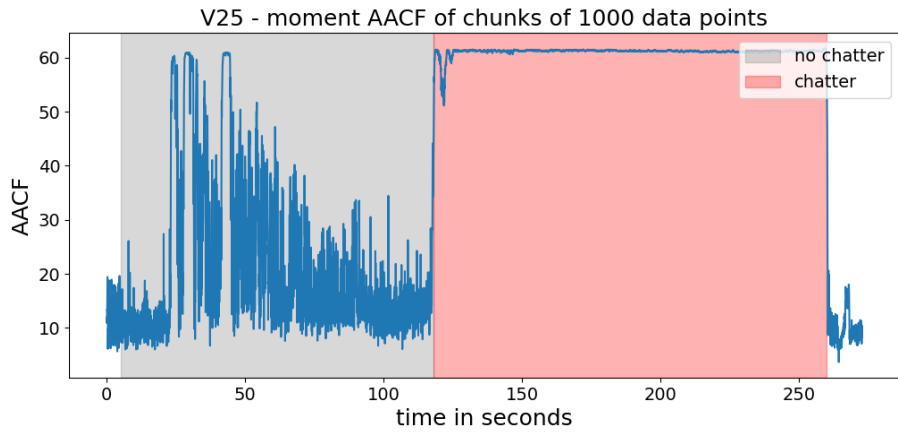Figure 19: *V24* process: A_{ACF} for *moment* variable

Figure 20: *V25* process: A_{ACF} for *moment* variable

If we were to stop the machine as soon as the A_{ACF} surpasses a value of 50, we are right in the beginning or the chatter in most cases. There is only one process, *V25* where A_{ACF} values greater than 50 occur during the *non-chatter* drilling time, without being closely followed by chatter. This can be observed in Figure 20.

We now want to determine if the high A_{ACF} values have predictive power that make a prediction leading up to the *chatter* region possible. It could also be that they only occur once we are already inside the chatter region, which would mean we would have to accept a bit of chatter before the machine can be stopped. Going by the cutoff rule of $A_{ACF} = 50$ we can now determine for each *V*-process at which point in time the threshold is surpassed for the first time. Table 4 shows when the threshold of $A_{ACF} = 50$ is surpassed for the first time for each of the 7 *V*-processes. Negative values in the second column indicate that the threshold was reached before being in the *chatter* segment.

Table 4: Time difference between the first point where $A_{ACF} > 50$ and start of *chatter* segment.

process	time	difference
V2	199.85 s	-0.15 s
V6	47.15 s	0.15 s
V10	47.15 s	0.15 s
V17	34.15 s	-0.85 s
V20	51.45 s	-0.55 s
V24	21.55 s	-0.45 s
V25	23.25 s	-94.75 s

Out of the 7 processes, 6 were able to locate the start of chatter within a tolerance window of 1 second. Only process *V25* gave a very early alarm (see Figure 20). The *D*-processes which used a damper, never show A_{ACF} values greater than 50, so the system does not seem to give false alarms if no chatter occurs at all. It is important to note that the exact value and sign of the difference should not be over interpreted, as long as it is in the sub-second range. This is because the beginning and end time points of *chatter* and *non-chatter* regions were determined manually by listening to the audio signal. It is hard to tell the *exact* point in time when chatter starts. We do not want to investigate the *low chatter* regions that were determined by the same method. The objective of this report is, to find out how to predict the start of the chatter. Splitting chatter into *chatter* and *low chatter* was only done to have more uniform time segments to analyze. The *cutting speed, feed speed* and *oil pressure* parameters do not seem to differ much between the *D*-processes (no chatter) and *V*-processes we have data for.

4 Summary and Discussion

In this report we analyzed time series data from 10 BTA deep hole drilling processes. 7 of these had audible chatter that we want to predict. We were able to show that out of all the variables, *moment* (drilling torque) showed the strongest difference between *chatter* and *non-chatter* regions. It is likely the best predictor variable for chatter as already found by Deistler and Scherrer (2022) and (Theis, 2004, p. 27). Next we found, that dividing the *moment* variable time series of each process into timed chunks with a length of 50 ms and calculating the A_{ACF} value for each chunk, we were able to state a cutoff rule, to detect chatter. The rule states that when $A_{ACF} > 50$ the machine should be stopped, because chatter occurs. This proved effective in 9 out of the 10 drilling processes we were given. The quality and usefulness of our findings is hard to gauge because we determined the labels (e.g. *chatter* regions) on our own. Having hard labels for chatter and spiraling in the data would have been better for our analysis. In total, our analysis was not able to prove true predictive power of the *moment* variable. The A_{ACF} indicator was able to give good indications of the start of chatter in most cases, however, it did not show any signs of chatter approaching in the seconds before the chatter was already there. Maybe it is enough though to stop the BTA machine as soon as the first signs of chatter appear. Our approach could however be a valuable alternative to listening to the acoustic signal manually in environments where there are a lot of acoustic disturbances. One point of contention in our approach could be the choice of the chunk size, as well as the number of lags used for the A_{ACF} calculation. In addition to monitoring the *moment* variable, using a damper is probably the best measure that can be taken to avoid chatter all together. We are not sure about what disadvantages a damper could have for the drilling process. If we had more data, other approaches could be taken to predict chatter and stop the machine early. Having only 7 samples of drilling processes that show chatter in the data, is also not enough to perform statistical testing, as most statistical tests require at least 30 samples. A Recurrent neural network that is fed the different variables in the time or frequency domain might be able to learn patterns that predict chatter. But we do not have enough data to test this approach. It would also be interesting to see if the A_{ACF} approach we chose in this report, could also work for different work piece materials and BTA tool diameters.

Bibliography

Botek Präzisionsbohrtechnik GmbH. BTA - System. `https://www.botek.de/en/deep-hole-drilling/bta-system/`, 2023. URL `https://www.botek.de/en/deep-hole-drilling/bta-system/`.

DAQLOG Systems Ltd. TEAC GX-1. `https://daqlogsystems.co.uk/product/teac-gx-1/`, 2023. Accessed: 2023-07-26.

Manfred Deistler and Wolfgang Scherrer. *Time Series Models*, volume 224. Springer Nature, 2022.

Michael Eid, Mario Gollwitzer, and Manfred Schmitt. *Statistik und Forschungsmethoden.* Beltz, 2017.

Tadeo Hepperle. gx1convert. `https://pypi.org/project/gx1convert/0.1.3/`, 2023.

John D. Hunter. Matplotlib: A 2d graphics environment. *Computing in Science & Engineering*, 9(3):90–95, 2007. doi: 10.1109/MCSE.2007.55.

pola-rs. polars: A python data manipulation library. `https://github.com/pola-rs/polars`, 2023.

Nils Raabe, Dirk Enk, Dirk Biermann, and Claus Weihs. Dynamic disturbances in bta deep-hole drilling: Modelling chatter and spiralling as regenerative effects. In *Advances in Data Analysis, Data Handling and Business Intelligence: Proceedings of the 32nd Annual Conference of the Gesellschaft für Klassifikation eV, Joint Conference with the British Classification Society (BCS) and the Dutch/Flemish Classification Society (VOC), Helmut-Schmidt-University, Hamburg, July 16-18, 2008*, pages 745–754. Springer, 2010.

Guido Van Rossum and Fred L. Drake. *Python 3 Reference Manual.* CreateSpace, Scotts Valley, CA, 2009. ISBN 1441412697.

Julius O. Smith. *Spectral Audio Signal Processing.* http://ccrma.stanford.edu/ jos/sasp/, 2023. online book, 2011 edition.

Winfried Theis. *Modelling varying amplitudes.* PhD thesis, Universität Dortmund, 2004.

UNISIG GmbH. What is bta drilling - unisig deep hole drilling machines. `https://unisig.com/information-and-resources/what-is-deep-hole-drilling/what-is-bta-drilling/`, 2023. Accessed: 2023-07-26.

VDI-Richtlinie 3210. Tiefbohrverfahren. Technical report, Beuth-Verlag, Berlin, 1996.

Klaus Weinert, Oliver Webber, M Hüsken, and Jorn Mehnen. Statistics and time series analyses of bta deep hole drilling. In *International Conference on Non-linear Dynamics in Mechanical Processing.* Citeseer, 2001.

Appendix

Starting on next page, because graphics are too large.
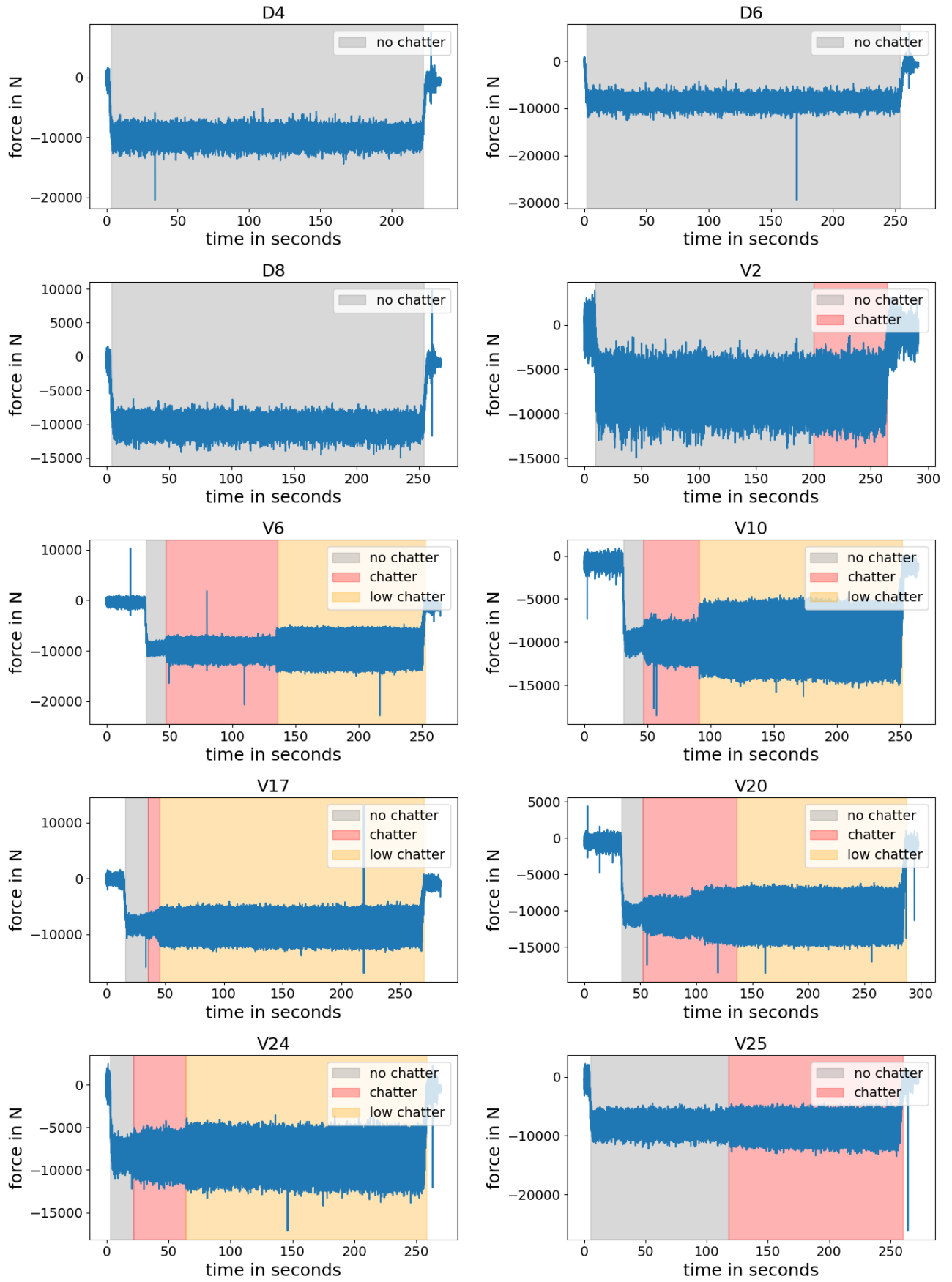
Figure 21: Force for all Processes

25
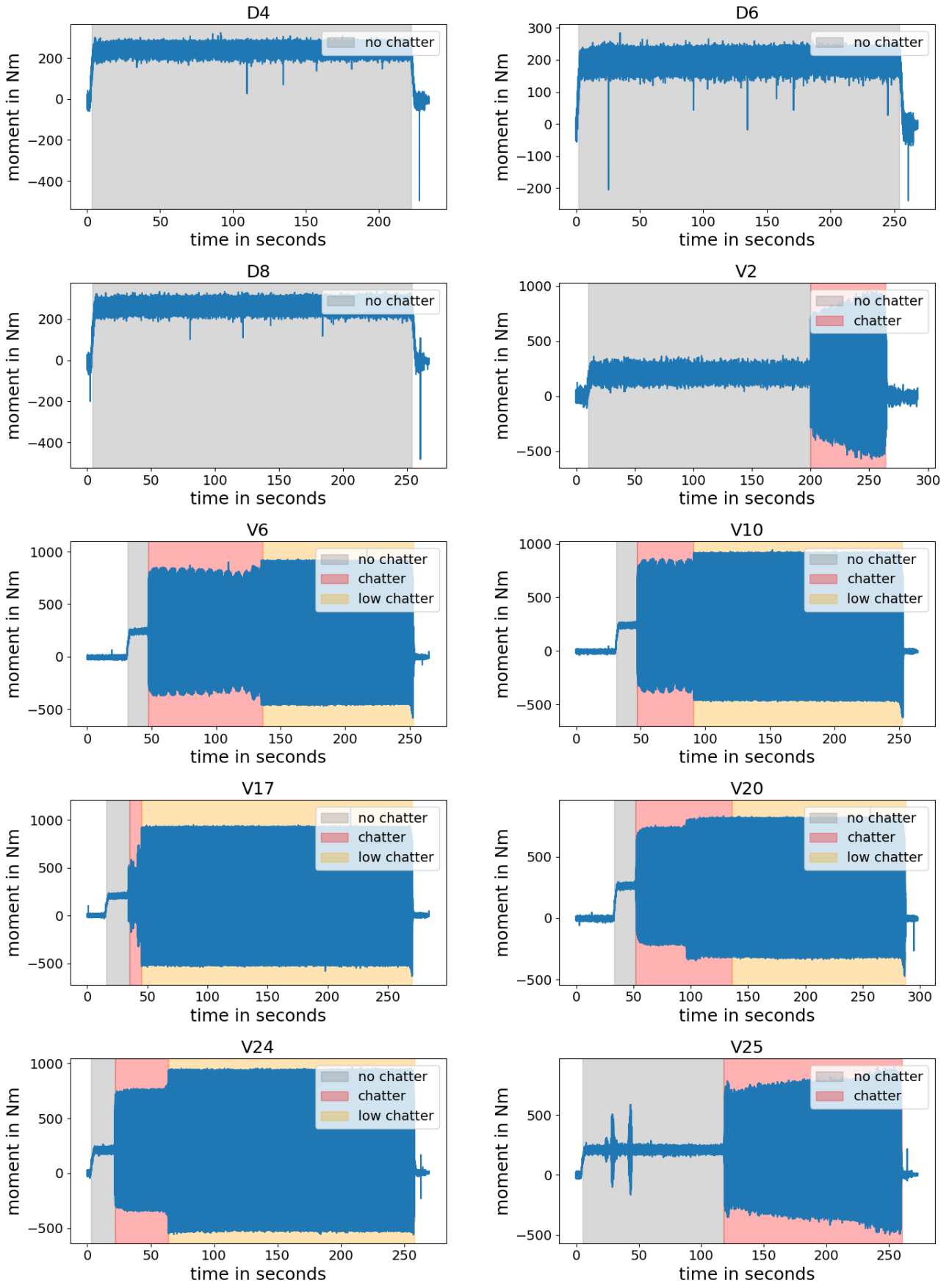
Figure 22: Moment for all Processes
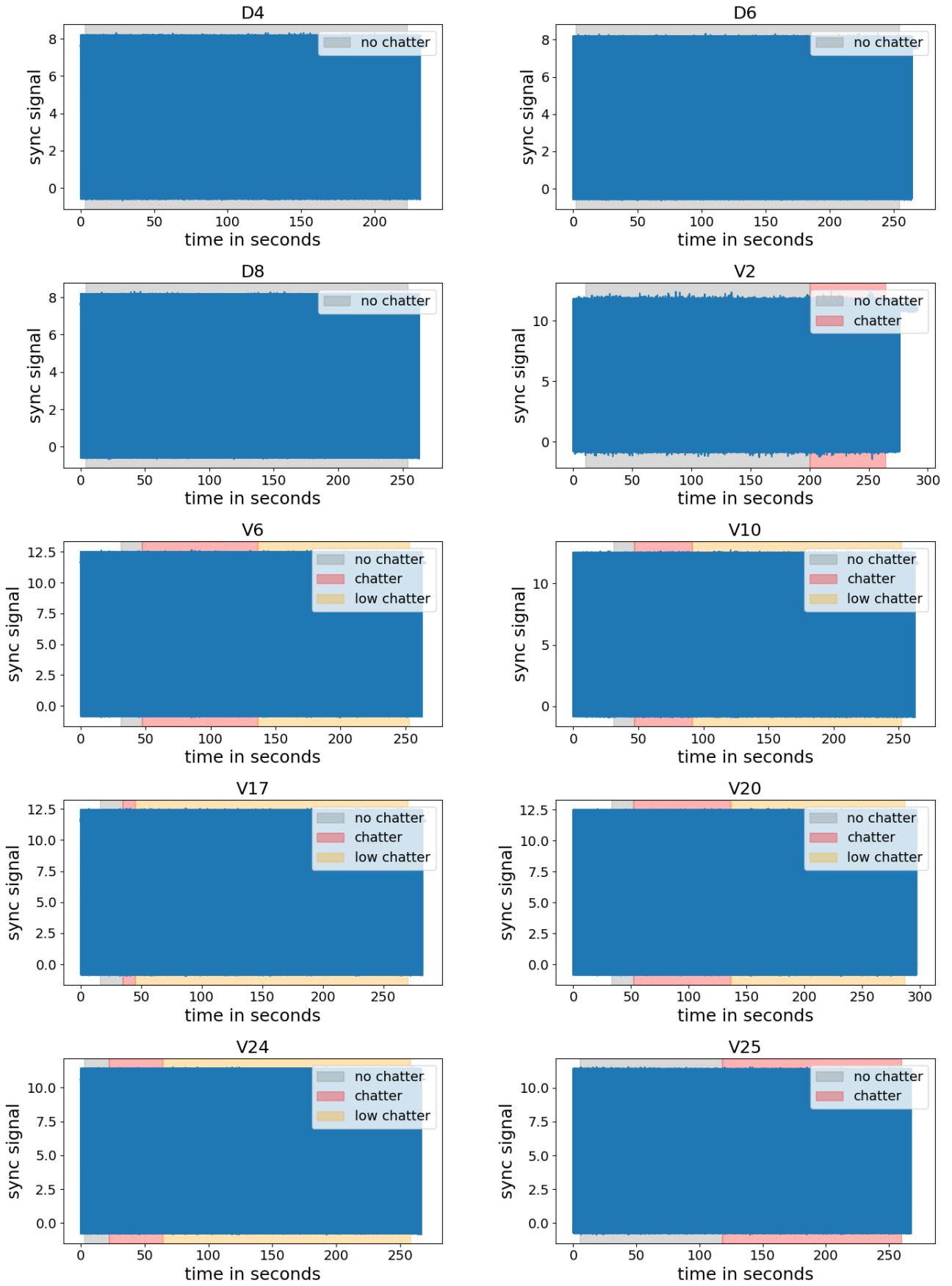
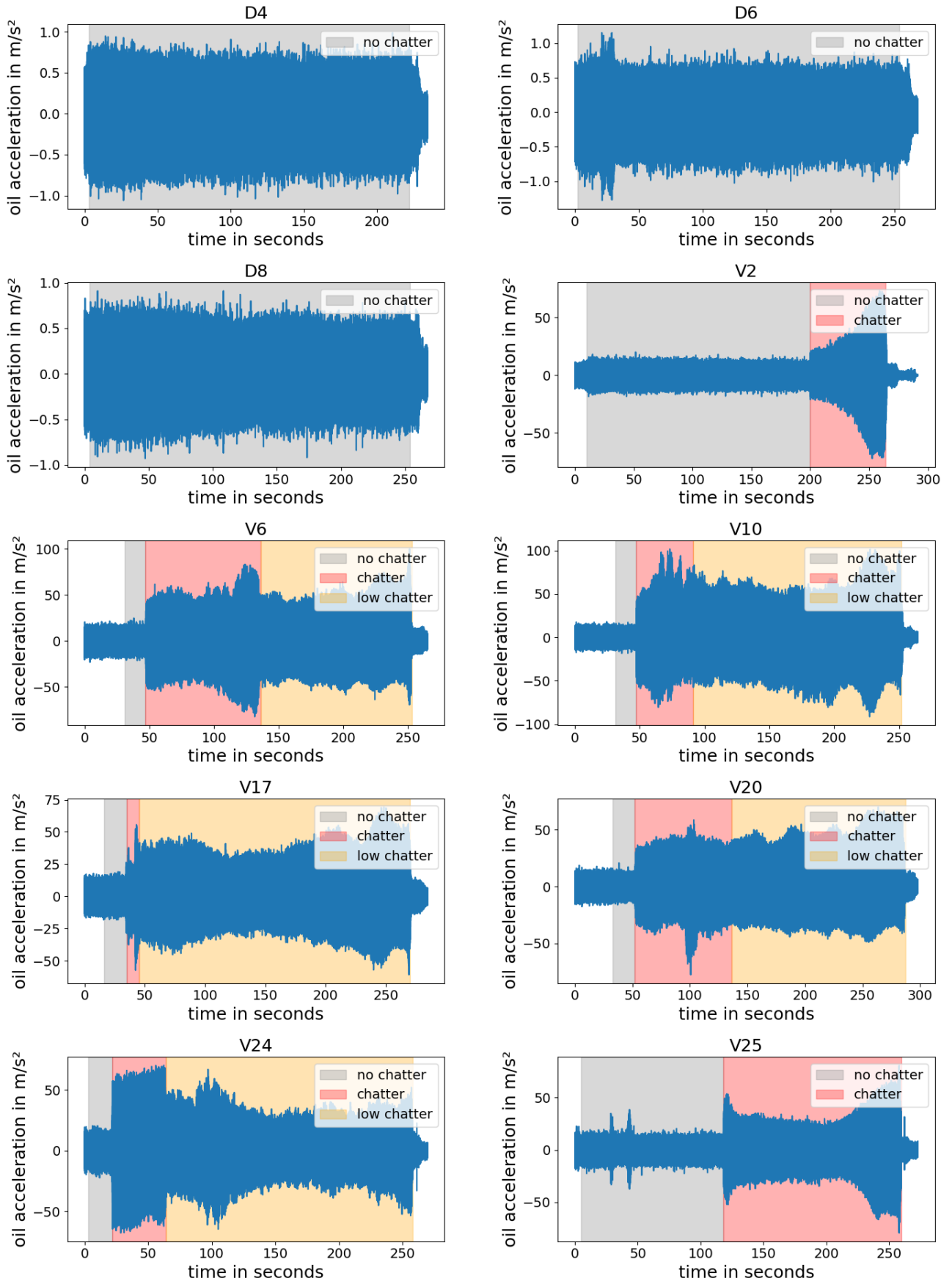Figure 23: Sync Signal for all Processes
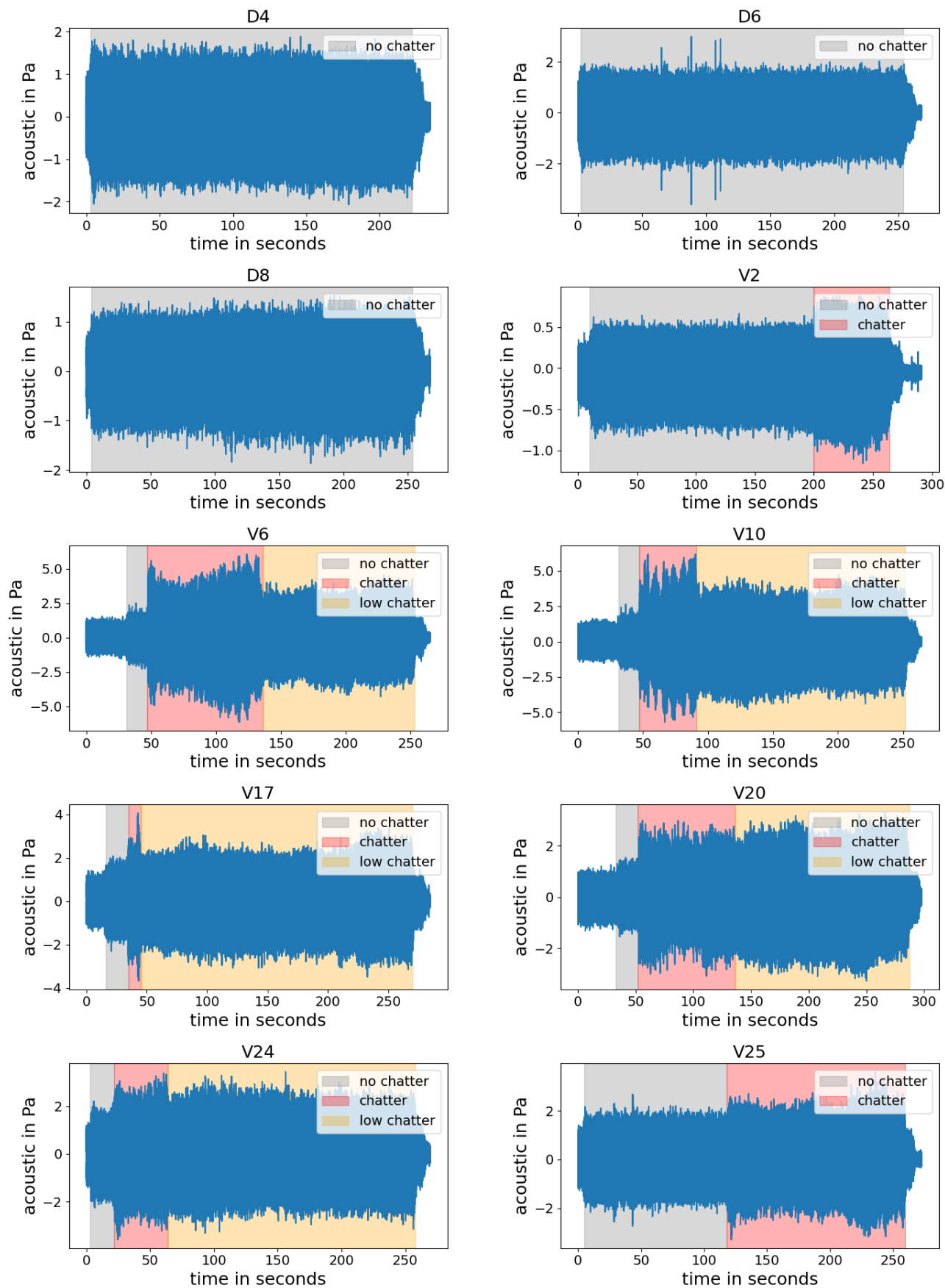
Figure 24: Oil Acceleration for all Processes

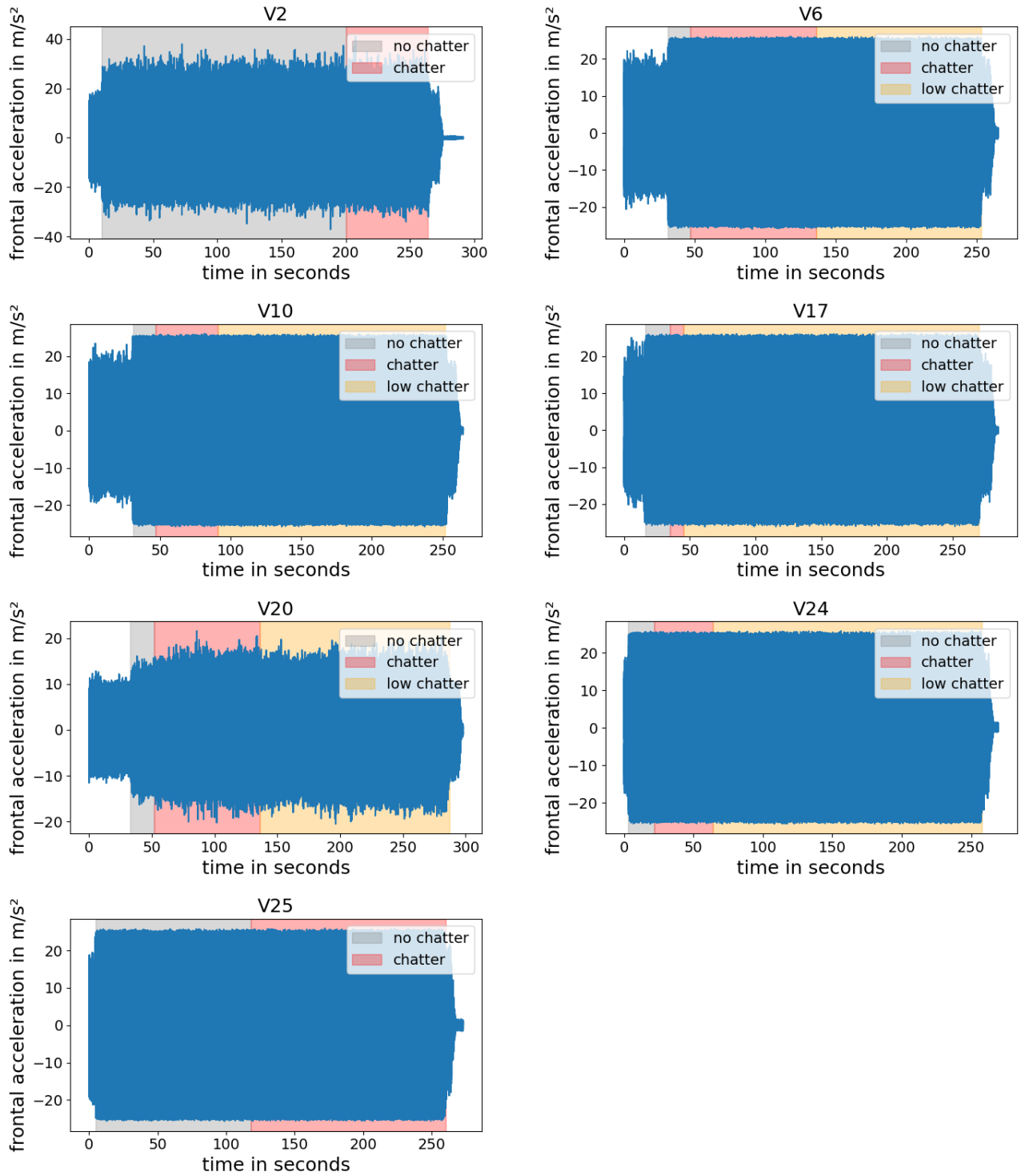Figure 25: Acoustic for all Processes
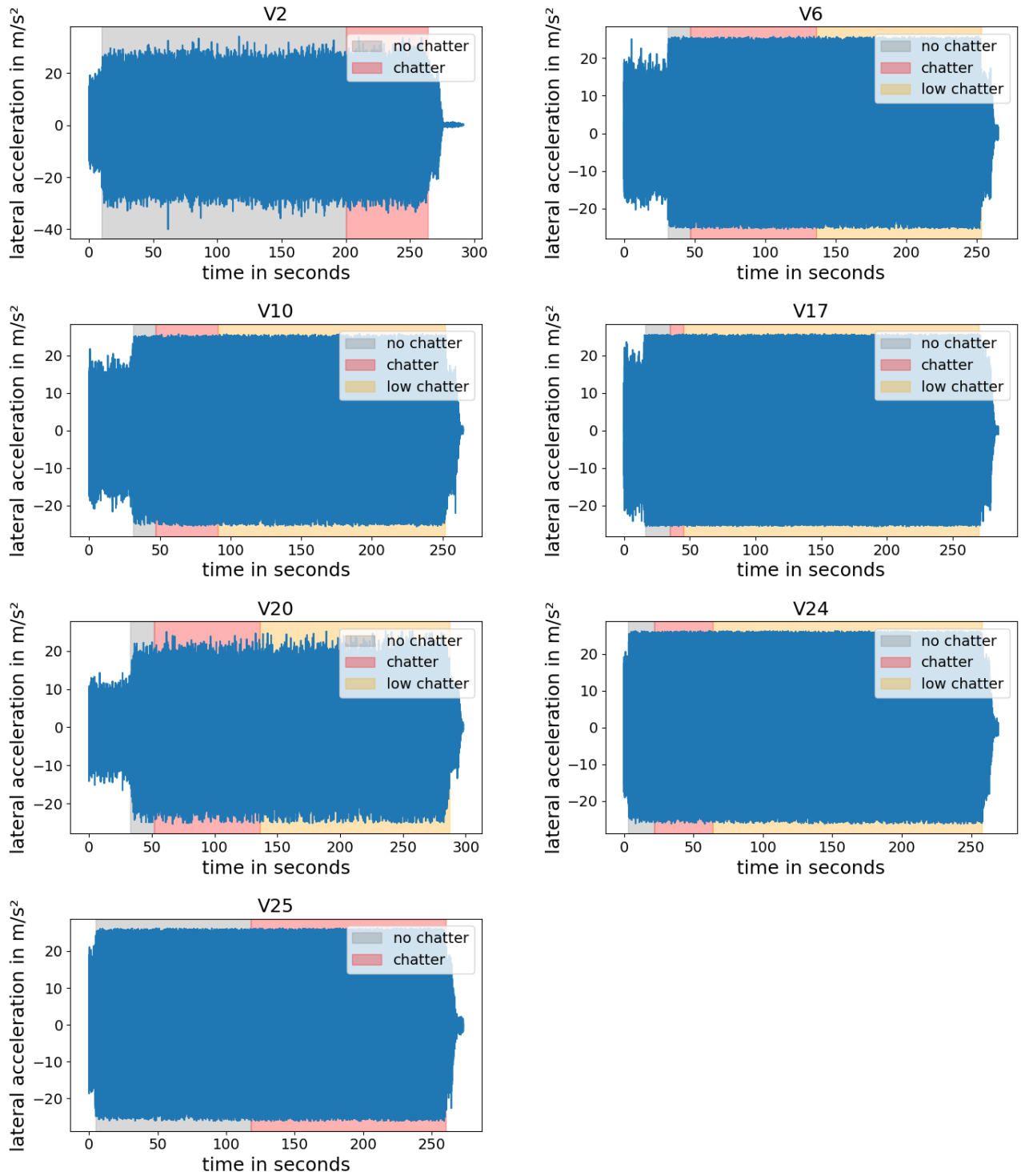
Figure 26: Frontal Acceleration for V-Processes

Figure 27: Lateral Acceleration for V-Processes